DYNAMIC MODELING AND THERMAL PERFORMANCE ANALYSIS OF A REFRIGERATED TRUCK BODY DURING OPERATION.

KEYWORDS: Road Transport; Refrigeration; Refrigerated Vehicle; Lumped Capacitance; Model

AUTHORS
Paolo Artuso[(1)], Antonio Rossetti[(2)], Silvia Minetto[(2)], Sergio Marinetti[(2)], Lorenzo Moro[(1)], Davide Del Col[(1)]

[(1)] Università degli Studi di Padova, Dipartimento di Ingegneria Industriale, via Venezia 1, 35131 Padova
[(2)] Consiglio Nazionale delle Ricerche, Istituto per le Tecnologie della Costruzione, Corso Stati Uniti 4, 35127 Padova

Abstract

The average cooling demand of a refrigerated vehicle depends on the external conditions and on the journey's profile, such as ambient temperature, air velocity, vehicle speed etc. In order to understand the dynamic heat load on the system and predict the peak of cooling demand, a fully dynamic model of the insulated box of a refrigerated vehicle was developed and experimentally validated. Experimental data was collected during test of a vehicle following the International Agreement for the Transport of Perishable (ATP) test. The model validation demonstrates the capability of the model to correctly predict the evolution of the internal box air temperature in both transient and steady-state conditions. The trend of dynamic load, peak of cooling demand, influence of the solar absorption coefficient and influence of the walls thermal mass on the cooling energy demand during a typical mission are also simulated.

1. Introduction

Energy consumption in the cold chain has been predicted to rise significantly in view of the increasing world population. In chilled and frozen food applications, temperature control during cooling, storage, transportation and display is essential to the maintenance of product quality. Refrigerated transport is an important link in the cold chain and refrigerated transport systems are widely used to distribute chilled and frozen products through the world while they are required to operate reliably in much harsher environment than stationary refrigeration systems, thus presenting a lower Coefficient Of Performance (COP)[1]. In addition to the low COP, increasing the quantity of transported goods, home delivery and expectations on the quality of goods bring to increasing the use of refrigerated transport systems, resulting in a tremendous amount of energy consumption by the refrigerated transport industry [1,2].
In a study presented by the United Nations Environment Programme (UNEP) [3] in 2010, an estimation of around 4 million refrigerated vehicles in service worldwide, including vans (40%), trucks (30%), semi-trailers or trailers (30%) was reported, forecasting by 2030 a growth by 2.5% a year of global road freight transport. A more recent document by Eurostat in 2017 [4] reported that the total number of refrigerated vehicle in Europe was superior to 4 million at the end of 2016, with an increase of 1.6% respect to the previous year. In view of the growing importance of the refrigerated transport sector, United Nations adopted an internal governmental Agreement on Transportation of Perishable food stuff (ATP). The agreement was signed in Geneva on 1 September 1970 and introduces common internationally recognized standards for temperature-

controlled transport vehicles such as road vehicles, rail wagons and sea containers, with the objective of facilitating international transport of perishable foodstuff while ensuring a high level of preservation during their carriage. The agreement establishes the appropriate temperatures under which the various types of perishable foodstuffs should be carried and also lays down the requirements for the equipment, as well as the methods and procedures for measuring and checking them [5]. According to the ATP standards, the insulating performance of a refrigerated vehicle is characterized by the overall heat transfer coefficient of its insulated body, K $Wm^{-2}K^{-1}$, which is measured in a climatic chamber. Below the value of 0.4 $Wm^{-2}K^{-1}$, vehicles are classified Reinforced Insulation (IR), while between the value of 0.4 and 0.7 $Wm^{-2}K^{-1}$ they are classified as Normal Insulation (IN). Despite the level of insulation of the refrigerated vehicle, thermal performance of the insulation material still deteriorates with time due to inherent foam characteristics [1]. Recent data showed a typical loss of insulation value between 3% and 5% per year which can lead to considerable rise in the thermal conductivity after few years [6,7], resulting in an significant increase in energy consumption and CO_2 emissions if the large number of refrigerated vehicle in use worldwide is considered. Furthermore, the value of the overall heat transfer coefficient of the insulated body can also be influenced by the manufacturing process: in a study provided by Estrada-Flores et al.[8] it was shown that for similar refrigerated vans the K -value can vary from 0.82 to 1.24 $Wm^{-2}K^{-1}$.

Energy consumption in the cold chain is still a global challenge and it is reported to account for 30% of total world energy consumption [9]. Despite the ATP regulation, road transport is responsible for a considerable part of global emissions: the percentage of CO_2 emissions caused by truck transportation in the European Union has increased from 5.6% in 1990 to 9% in 2014, causing 14% of global emissions [10]. In 2016, Adekomaya et al.[11] stated that 15% of world's energy from fossil fuel is used in food transport refrigeration, and the environmental influence of emissions form food transport vehicles account for 40% of the global greenhouse effect. After all, diesel engine driven vapour compression system account for huge fuel drain in transport refrigeration systems and by today is the most common refrigeration system in use, with an expected coefficient of performance generally between 0.5 and 1.5 [1]. A typical refrigerated vehicle cooling system interacts with the truck cargo space and regulates the space condition to a certain temperature by extracting the heat from the cargo and transferring it to the external ambient environment. In refrigerated transport, methods for modulating refrigeration power to part-load operations include hot gas bypass, suction throttling, compressor on-off and compressor speed control [12].

Compressor speed control, either in stages or continuously through an inverter supply, is effective but is limited in its unloading capacity and needs an additional control method to reach low levels. By far, the most common temperature control in the refrigerated transport having a cooling unit based on a vapor compression cycle is a simple on-off feedback controller with hysteresis [13] where the compressor's on or off control action is driven by the difference between measured cargo space temperature and set-point temperature. To investigate and improve the refrigeration system performance, good knowledge of the system behavior is required: this knowledge can be obtained from modelling and simulation tools or through experimental studies. Numerical modelling offers and economic alternative to physical experiments, though a reliable model needs to be validated with experimental data.

Literature review shows that different authors have reported various studies presenting numerical models of refrigerated transport system in order to evaluate the system's performance during operation: Jolly et al.[14] developed a mathematical model to simulate the steady state performance of a shipping container refrigeration system. Sub models of compressor, evaporator, condenser and thermostatic expansion valve

were created and later coupled by appropriate mass and energy transfer relation to form the full model. The model proved to be useful in the performance evaluation of different refrigerant in such systems but being in steady state conditions it was unable to evaluate the effect of the dynamically changing of external ambient conditions. Li et al.[15] considered the varying ambient temperature and developed a dynamic numerical model of the insulated body of a refrigerated vehicle coupled with the numerical model of a cooling unit, implementing an optimization algorithm in order to investigate on the optimal temperature bounds to regulate the cargo space temperature. The same authors later used the same numerical model to study the transient behavior of the cooling system during cooling/heating-mode switch cycling operations [16]. Tso et al.[17] developed a mathematical model of the refrigeration unit in a typical electricity-driven refeer, which considered the effects of hot gas bypass and suction modulation control on performance in partial load, but lacked a validation because of absence of experimental data and was restricted to steady state conditions. S.K. Chatzidakis et al.[18] studied a dynamic model based on a transient finite difference method to simulate a classical ATP test chamber coupled with a typical specimen refrigerated vehicle to be tested. The same authors also modelled the isothermal tanks that are widely used for the transport of perishable liquid foodstuffs like milk, wine, juice, etc… [19].

In majority of food refrigeration systems, heat is transferred primarily by convection: air temperature and its homogeneity are directly governed by the patterns of airflow. Different studies have shown a significant level of spatial temperature variability in some food refrigeration systems [20,21,22] with non-uniform airflow as a major cause of this variability. The air distribution system must provide sufficient airflow to absorb energy from heat sources as walls, door and often products itself to avoid unacceptable temperature increase: the optimizing of these systems is not an elementary problem and may require extensive experimentations. For this purpose different authors made use of computational fluid dynamics (CFD) simulations to study the characteristics of airflow inside of the insulated body of a refrigerated vehicle[23,24]. Furthermore, temperature spatial variability is also affected by the frequent door openings refrigerated food vehicles are subject during their travel. In a survey carried by James et.al [13], the author stated that small-refrigerated vehicles that conduct multi-drop deliveries can be subjected to as many as 50 door openings, where there is heat ingress directly from outside and from personnel entering to select and remove products.

Tso et al.[25] used a commercial CFD program and modelled the heat and mass transfer during the door openings of a refrigerated vehicle, studying the impact on the internal space air temperature. A series of experiments was carried out to study the effect of door openings with unprotected doors, with air curtains and with plastic strip curtains. The CFD simulations generally overestimated the temperature rise by between 3 and 4 °C which was believed to be due the effect of condensing water vapour in experimental situation. Moureh et al.[26] used Fluent with RSM turbulence model to predict the airflow pattern with a 3-D configuration of a typical refrigerated vehicle loaded with two rows of pallets. Later on, Moureh and Flick[27] used the numerical approach developed in the previous study to characterize the influence of an air-duct system and the narrow air space separation (1-2 cm) between pallets and walls. Tapsoba et al.[28] also used CFD with the RSM turbulence model to predict the 3-D airflow pattern within a refrigerated vehicle, with and without an air-duct system, loaded with two rows of slotted pallets.

While a lot of effort is used in modeling the internal air flow pattern and the cooling system performance, only few study focused on the development of a reliable dynamic model of the refrigerated body, even though it is a key element to relate the external loads to the actual heat flow on the insulated body internal surface.

For example, Estrada-Flores [29,30] discussed the dynamic response of diverse insulating walls, comparing different 1D numerical models approaches. Lumped models of a layered insulating wall were demonstrated inferior to Finite Elements Methods (FEM) discretization when dynamic response accuracy was considered. Despite the good capability of FEM to reproduce both steady and dynamic response, the presence of local thermal bridges and irregularities [31], such as structural elements or plate anchors inside the layered wall force the use of a full 3D model to obtain reliable results.

This paper presents a novel approach to model the average transient response of the insulated body. A 0-D lumped parameter model is used to characterize the refrigerated box structure. The model is tuned and successively validated over experimental data. In this way, the actual performance of the structure can be reproduced without the need for the detailed drawing of the structure or the knowledge of the actual properties of the material used for the construction.

The model is then applied to evaluate the cooling demand of the insulated body of a refrigerated truck body during a transport mission.

After the description and validation of the numerical model, the paper provides also simulations of a one-day typical mission with the analysis of the main thermal fluxes that condition the cooling power demanded by the vehicle and the dynamic load that insists on the external surface of the structure. A study of sensitivity of the model to a variation of surface absorptivity and wall thermal mass of the truck body was performed, making consideration on the variation of cooling energy demanded during the mission.

2. Experimental characterization of the present study case

A refrigerated truck body with an internal air volume of 9.75 m^3 has been considered and experimentally characterized in the present study. The considered truck body was produced by ISOKIT s.r.l. and tests were performed less than one month after the end of the production.

Based on widespread technology, walls are made up of three layers consisting of a polyurethane foam sandwiched between two thin fiberglass-based layers, reinforced with wooden and metallic structural component as needed to obtain the requested sturdiness. The floor includes an additional layer of plywood plate, necessary to meet the requested mechanical resistance. Complete stratigraphy of the walls is presented in Appendix 1. The cooling unit's maximum power was chosen from a commercial catalogue by Carrier [32]. The nominal cooling capacity at 0°C and 30°C internal and external temperature respectively, as well as the main external dimensions of the vehicle are shown in Table1. In the table the total internal and external surface that account for the 6 walls of the insulated body are also reported.

Table 1: Main external dimensions of the insulated box.

$\boldsymbol{H_e}$ [m]	2.0
$\boldsymbol{L_e}$ [m]	3.0
$\boldsymbol{W_e}$ [m]	2.0
$\boldsymbol{S_e}$ [m^2]	32.0
$\boldsymbol{S_i}$ [m^2]	27.9
$\boldsymbol{V_i}$ [m^3]	9.75

$\dot{Q}_{c\,nom}$ [W] (T_i =0 °C , T_{amb} = 30 °C)	2575

The truck body was first investigated under steady state conditions, to quantify its global heat transfer coefficient K, as defined by ATP agreement. The test took place at the ATP test station, located at The Construction Technology Institute of the National Research Council in Padova, following the Annex 1 of the ATP guidelines [5]: a representative scheme of test station and insulated truck body during a typical test is provided in Figure 1.

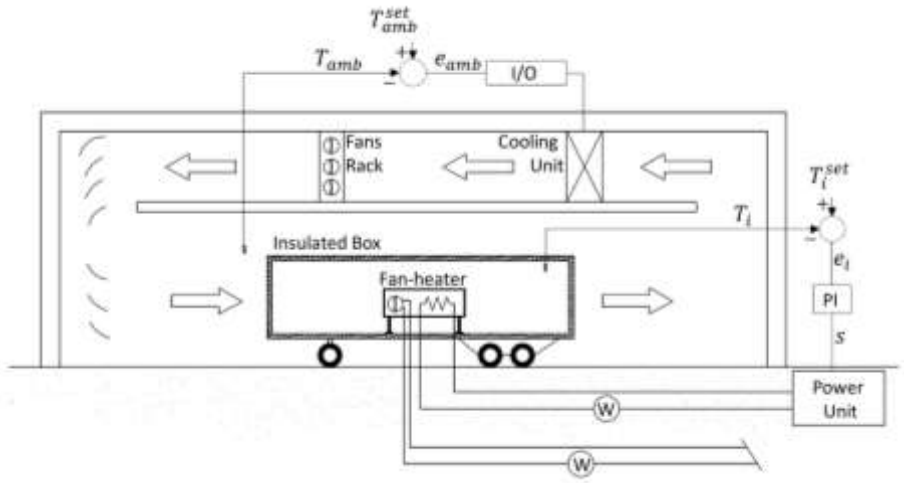

Figure 1- Scheme of ATP test station and refrigerated semitrailer during a typical ATP test.

The testing method is based on imposing a known and controlled thermal load by electrical heating inside of the insulated box through the use of fan-heaters. The temperature constraints are given for both the internal and external air temperature; each of those is measured on 12 prescribed points located at 100 mm from the body walls. As the temperature difference should be maintained in the 25 °C ± 2 °C range, while the mean temperature between inside and outside is 20 °C ± 0.5 °C, the external outside air temperature was set to $T_{amb} = 7.5$ °C while $T_i = 32.5$ °C was set for the internal air. The fan-heaters, responsible for the heating capacity are controlled with a PID controller imposing the set internal temperature of 32.5°C. The facility's cooling unit, coupled with a fan-group is responsible for the external temperature and ventilation in the range 1-2 $ms^{-1,}$ as prescribed by the ATP guidelines [5].
Accuracies of the instruments employed during the experimental test and on the measured global transfer coefficient K are summarised in Table 2.

Table 2: Uncertainties of instruments.

INSTRUMENT AND PARAMETERS	ACCURACIES
Thermocouple	± 0.2 K
Length meter	± 0.02 m
Electrical power meter	$\pm 2\%\ \dot{Q}_H$
Uncertainties on global heat transfer coefficient	$\pm 4.7\%$

The trend of the heating power supplied by the fan-heaters during the test is presented in Figure 2a. During the initial part of the test, the heating power is set to its maximum level by the controller, corresponding to

$\dot{Q}_{h,nom} = 1700$ W. As the difference between the measured internal air temperature and the set-point temperature of 32.5°C decreases, the PI controller modulates the value of the heating power until it reaches a steady state value of 270 W, once the set-point temperature has been reached.

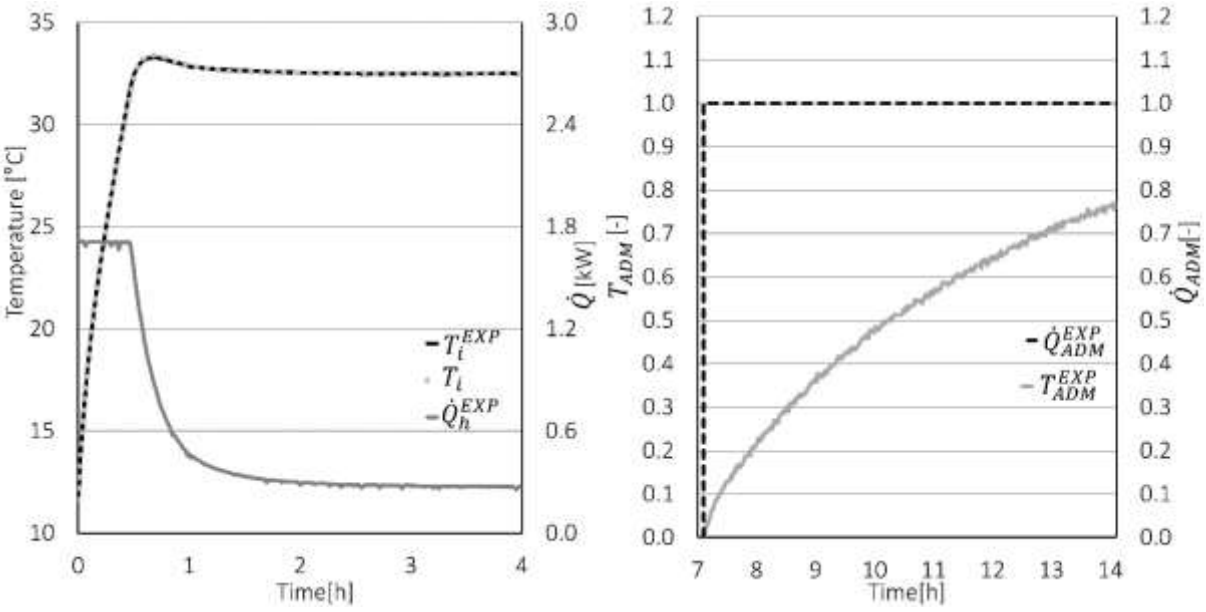

(a) (b)

Figure 2- a) Experimental value of $\dot{Q}_h$ and T_i during the ATP test. b) Experimental trend of the non-dimensional temperature T_{ADM} during the step test .

The steady state condition is reached for this test after 3 hours from the beginning of the test, assuming as reference for stability a drift of the heating power less than 3 % in one hour. The global heat transfer coefficient K is then calculated according to:

$$K = \frac{\dot{Q}_h}{S_m\,|T_{amb} - T_i|} \tag{1}$$

where the values are averaged over a 30 min period, once the steady state condition is achieved. A value of 0.36 W m^{-2} K^{-1} for the insulated body was evaluated, thus classifying the refrigerated truck body as heavily insulated equipment (K≤0.40 W m^{-2} K^{-1}) according to the ATP standards body types. After 7 hours from the beginning of the test, 4 of which under stable conditions, a step test, where a sudden increase in heating power is applied, was performed to document the dynamic response of the system. A sudden increase in the heating power with reference to the test conditions was imposed. In the step test, the temperature is expressed in non-dimensional terms, T_{ADM}, defined as:

$$T_{ADM} = \frac{T_i - T_i'}{T_i'' - T_i'} \tag{2}$$

Where T_i' is the value of the internal air temperature in the steady state conditions before the step test and T_i'' is the value of the internal air temperature in the new steady state condition achieved after the step, being the new heating power $\dot{Q}_h''$.

The trend of the non-dimensional temperature T_{ADM} is presented in Figure 2b: during the test, it has been observed that the transient region in which the air is responding dynamically can be divided into 2 sub-zones: a first zone where the system responds rapidly to the increase of power and a second zone where the system responds slowly (which also happened to be the dominant one in the long run). Since the slow response is the dominant one in terms of time, it was chosen as the one representative of the test and the trend of the experimental process reaction curve can be approximated as a first order linear system response with a characteristic time of 5.1h.

3. Model description and tuning

3.1. Numerical model set-up

In order to develop a simple and reliable numerical model able to correctly reproduce the dynamic thermal behavior of the system composed by the insulated body walls, the internal air and the additional equipment or goods inside of the box, a lumped capacitance zero dimensions transient modelling method was chosen, solving for the node temperatures as a function of time

The whole insulated box was modelled as a 0-D model defined by a series of resistances and capacities. With the aim of increasing the capability of the equivalent formulation to reproduce the actual average response of the insulated box, thus including the impact of both distributed and localized effects on the average internal temperature, a series of lumped resistance and capacities was used. The extreme nodes of this series represent the internal and external average surface temperature of the box. In the present case, preliminary studies, demonstrated that the use of 12 capacities ($C_0, \dots, C_{11}$) and 11 resistances ($R_1, \dots., R_{10}$) were enough to reproduce the experimental response of the box, as presented later section 3.2. The insulated box model is presented in Figure 3a.

The total structure thermal resistance and thermal capacity are then calculated as the algebraic sum of the components:

$$C_w = \sum_{j=0}^{11} C_j \tag{3}$$

$$R_w = \sum_{j=1}^{11} R_j \tag{4}$$

Using a thermal-electric circuit analogy, the whole system can be represented with a thermal network composed of electrical resistance and capacitance, as can be seen in Figure 3b, which provides a better illustration of the heat transfer phenomena taken into account in the system.

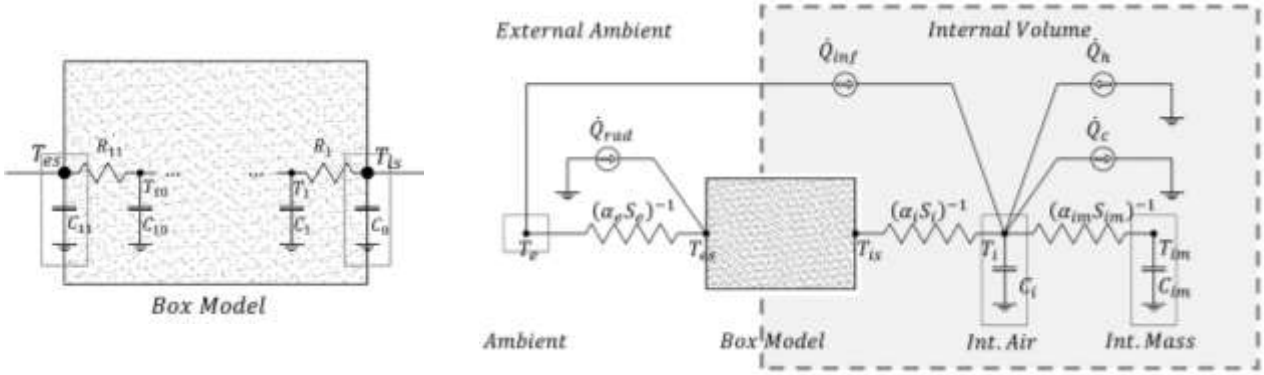

(a) (b)

Figure 3- Thermo-electric circuit analogy of the system: (a) Insulated box model; (b) internal and external elements.

The model on the external side account for the convection and radiation exchanges, insisting on the average external surface temperature T_{es}. The average air volume, at temperature T_i, is instead influence by the infiltration load ($\dot{Q}_{inf}$), heating or cooling power ($\dot{Q}_h$, $\dot{Q}_c$) and convection with the internal wall temperature. A further convection term was considered to model the exchange between the air and other capacities inside the box, such as heating or cooling equipment or transported goods, represented by the capacity C_{im} at temperature T_{im}.

The linear differential system defined by Eq.s 5-9 provides the energy balance of the internal air (Eq. 5), the interior and exterior surface heat balance governing equations (Eq. 6 and 8 respectively), the equivalent refrigerated box model thermal balance (Eq. 7) and the energy balance between the internal air and the internal mass (Eq.9).

$$C_i \frac{dT_i}{dt} = \left(\dot{Q}_h - \dot{Q}_c\right) + \alpha_i S_i (T_{is} - T_i) + \alpha_{im} S_{im} (T_{im} - T_i) + \dot{Q}_{inf} \quad (5)$$

$$C_0 \frac{dT_{is}}{dt} = \alpha_i S_i (T_i - T_{is}) + \frac{1}{R_1}(T_1 - T_{is}) \quad (6)$$

$$C_j \frac{dT_j}{dt} = \frac{1}{R_{j+1}}\left(T_{j+1} - T_j\right) + \frac{1}{R_j}\left(T_{j-1} - T_j\right) \ , \ j = 1 \dots 10; \text{ with } T_0 = T_{is} \text{ and } T_{11} = T_{es}; \quad (7)$$

$$C_{es} \frac{dT_{es}}{dt} = \frac{1}{R_{11}}(T_{es} - T_{10}) + \alpha_e S_e (T_{amb} - T_{es}) + \dot{Q}_{rad} \quad (8)$$

$$C_{im} \frac{dT_{im}}{dt} = \alpha_{im} S_{im} (T_i - T_{im}) \quad (9)$$

The convective heat transfer coefficient α_i is assumed to have a constant value deduced with measurements of the internal surface temperature during the ATP test (see section 3.2), while on the external surface the convective heat transfer coefficient α_e is computed from a convection over a plate correlation [33], due to its dependence to the vehicle velocity during operation. The conductive resistance of the wall is considered as a unique conductive resistance for the whole insulated body R_w, accounting for the overall insulating capacity of the box.

$\dot{Q}_{rad}$ is the net solar gain (Eq. 10), given by four different contribution: the direct solar radiation, the diffusive incident solar radiation, the radiation heat exchanged between the surface and the sky and between the surface and the ground [34]:

$$\dot{Q}_{rad} = \sum_{u=1}^{6} S_u \left[a_s \left(\vec{I}_{dir} \cdot \hat{n}_u + I_{diff}\right) + \sigma\varepsilon \left(\frac{(1+\hat{n}_u \cdot \hat{k})}{2}\left(T_{sky}^4 - T_{es}^4\right) + \frac{(1-\hat{n}_u \cdot \hat{k})}{2}\left(T_{amb}^4 - T_{es}^4\right) \right) \right] \quad (10)$$

where u=1..6 refers to the six external surfaces and their respective orientation $\hat{n}_u$ and $\hat{k}$ is the normal vector toward sky globe . Truck orientation was assumed to be constant with respect to the solar radiation, with the front of the refrigerated box normally oriented North. The fictive sky temperature is calculated by assuming the sky to be an ideal black surface and can be determined by [35]. Assuming an unpainted Glass-Fiber

Reinforced Plastic (GFRP) surface, surface absorptivity a_s was set to 0.15, and surface emissivity ϵ was set to 0.90 according to [36].

The infiltration heat load $\dot{Q}_{inf}$ is given by the leakage of outside air into the insulated body during the opening of the vehicle's doors or due to the imperfect seal of the doors during operation: the volumetric flowrate $\dot{V}_{inf}$ of external air entering the vehicle body is modelled after the study of T.lafaye de Micheaux et al.[37]. During the door opening operation the volumetric flowrate $\dot{V}_{inf}$ is evaluated assuming an instantaneous and complete door opening while during transportation, when the door is closed, the volumetric flowrate entering the internal space corresponds to an air change per hours of 0.02 h^{-1} [15], , which correspond to $\dot{V}_{inf} = 0.02\ [h^{-1}]\ V_i$.

$\dot{Q}_h$ and $\dot{Q}_c$ represent respectively the heating and cooling thermal sources inside the insulated box. The control system is modelled for both the heat sources as a PI control with output $s \in [0..1]$. A simple anti wind-up scheme was implemented to limit the maximum values of the integral part. The PI controller logic is presented in Figure 4.

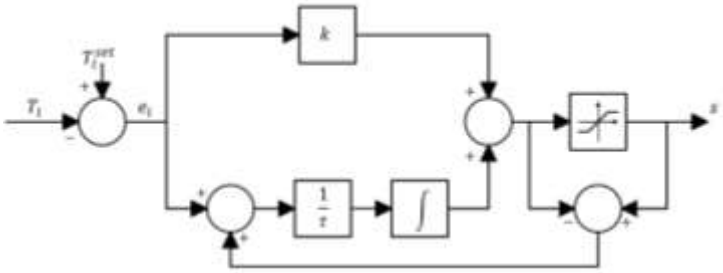

Figure 4-PI controller scheme.

3.2. Tuning of the numerical model

The parameters required as input to the numerical model are the thermal capacity and thermal resistance of the walls. Initially these values were assumed from the average wall thickness and composition of the insulated box walls. The value of 632.3 kJ K^{-1} for the total wall thermal capacity was computed from the average wall composition, assuming for the polyurethane foam $C_p^{foam} = 1450$ J kg^{-1} K^{-1}; $\rho^{foam} = 35$ kg m^{-3} and $C_p^{f.glass} = 1260$ J kg^{-1} K^{-1} $\rho^{f.glass} = 1700$ kg m^{-3} for the fiberglass as follow:

$$C_W^{av} = \sum_{t=1}^{n} S_t \delta_t C_{p,t} \tag{11}$$

where t refers to the generic layer composing the walls of the insulated body. The value of 863 10^{-4} K W^{-1} for the thermal resistance R_w^{av} of side wall of the truck body was experimentally measured by means of heat flow meter apparatus on a 500mmx500mmx70mm samples. This apparatus allows determination of the thermal resistance with an accuracy of 2%.

Figure 5 provides the trend of temperature prediction (Figure 5a) and the difference between simulated and experimental value of internal air temperature (Figure 5b) if the average wall characterization were to be used to characterize the equivalent refrigerated box model in equations 5-9, given as input the heating power $\dot{Q}_h$ measured during the experimental activities reported in section 2.

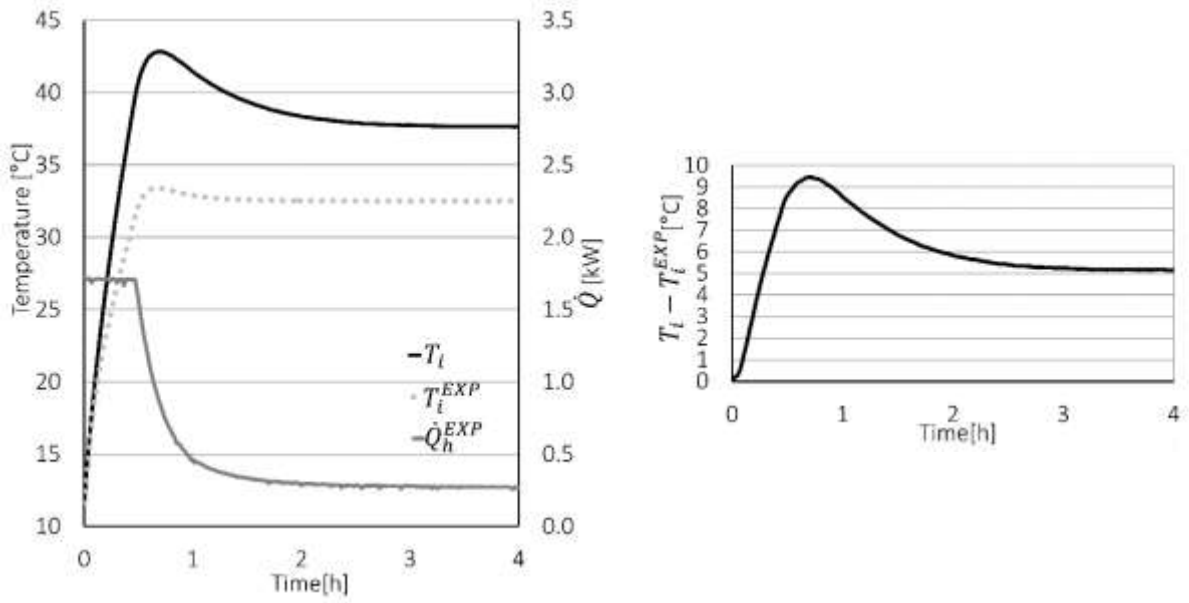

(a) (b)

Figure 5- a) Experimental value of $\dot{Q}_h$ and T_i and simulated values obtained using thermal mass and resistance from the experimental wall characterization. b) Difference between simulated and experimental inside temperature ($T_i - T_i^{EXP}$) for the refrigerated truck body.

It can be observed that the steady state condition is achieved at 37.6°C instead of 32.5°C and the maximum difference between temperature prediction and experimental value is equal to 9.5 °C during the dynamic evolution of the internal air.

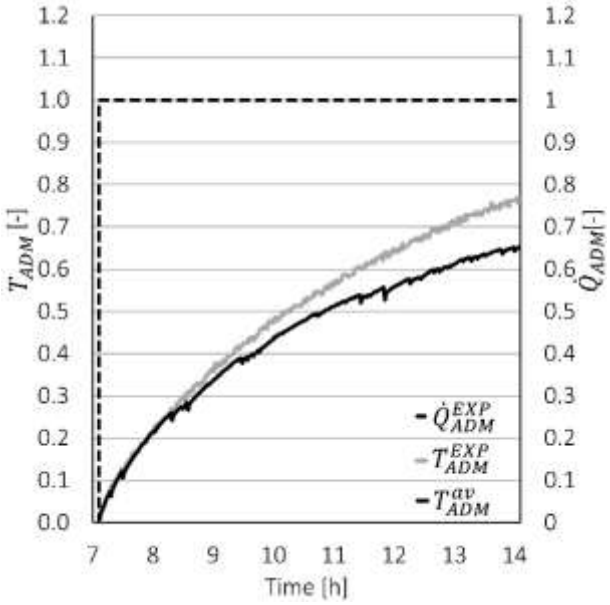

Figure 6- Step response of the system to a sudden increase of heating power: comparison between experimental data and simulated data using the thermal properties obtained by the average wall composition.

Similar results are obtained in the simulation of the step-response (Figure 6) using the thermal properties evaluated from the average wall thickness characterization: it can be observed that the non-dimensional

trend of the step response is slightly different from the experimental trend, having a characteristic time of 7.4h instead of 5.1h.

This confirms that the overall thermal capacity as well as the insulation characteristics cannot be derived from the wall average composition (i.e. stratigraphy), since a great part of the insulated box mass is made by wooden and metal localized reinforcement.

The data collected during experimental activity were used to tune and validate the model in both dynamic and steady-state conditions. The use of experimental data allowed to obtain a reliable model, avoiding the need for detailed description of the box structure and materials, and the resolution of a 3D thermal model accounting for all the thermal pairs and bridges of the structure.

The value of the wall's thermal capacity C_w and conductive resistance R_w were then optimized to fit experimental data. Others variable optimized were the thermal capacity C_{im} and the convective heat loss factor $\alpha_{im}S_{im}$ of the internal mass inside of the insulated box, i.e. internal cladding of the walls, fan-heaters and evaporator, which were included into the model as the internal mass of equation 9. The optimal value of this 4 parameters has been found through formulation of an optimization problem in Matlab[38] aimed at minimizing mean quadratic error between the measured and simulated temperature of the internal air during the test. These 4 lumped parameters represent the equivalent values of the physical parameter to be used in the lumped model in order to catch the real behavior of the truck body.

$$\text{Find } [C_w\ R_w\ C_{im}\ (\alpha_{im}S_{im})] \text{ which minimize } MSE = \frac{\int_0^{tmax}(T_i - T_i^{EXP})^2 d\tau}{t_{max}} \tag{11}$$

under the following constraint: $\dot{Q}_h(t) = \dot{Q}_h^{EXP}(t)$; $T_{amb}(t) = T_{amb}^{EXP}(t)$;

Table 3: Numerical model's optimum parameters.

PARAMETER	DEFINITION	TRUCK BODY	
$\boldsymbol{C_w}$	Wall thermal capacity	632.3	kJ K^{-1}
$\boldsymbol{R_w}$	Wall resistance	863 10^{-4}	K W^{-1}
$\boldsymbol{C_{im}}$	Internal mass thermal capacity	29.6	kJ K^{-1}
$\boldsymbol{\alpha_{im}S_{im}}$	Internal mass conductance	371.8	W K^{-1}

The prediction of internal temperature by the model was compared with the experimental data (Figure 7a), finding that the model results are in an excellent agreement with the experimental temperatures and getting a maximum difference between simulated and experimental internal temperature lower than 0.3°C (Figure 7b).

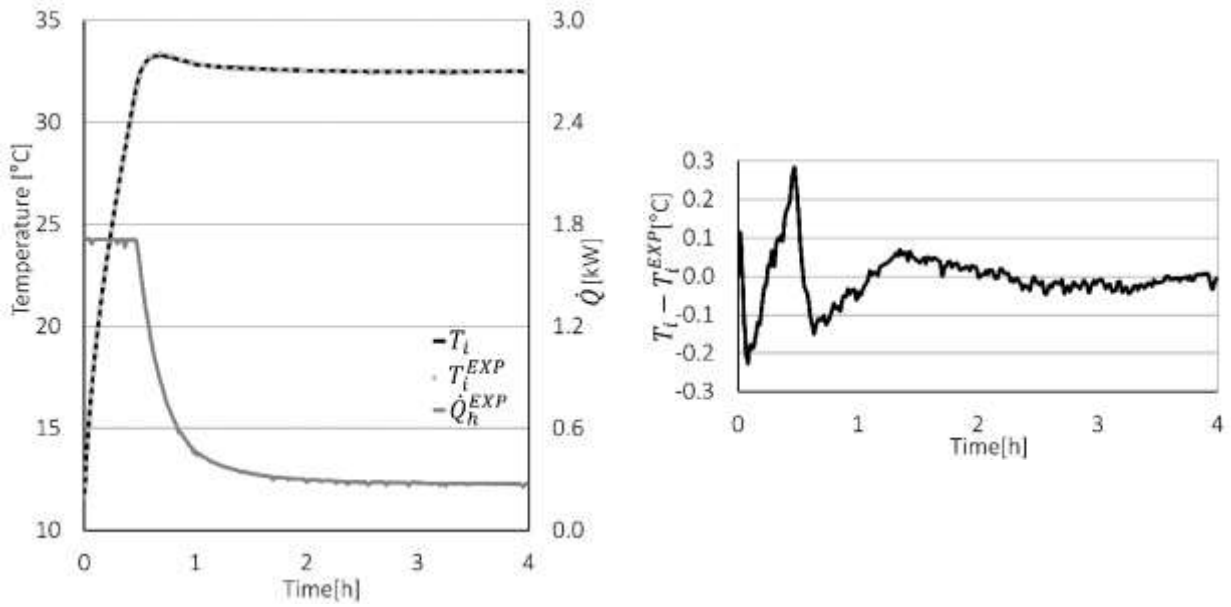

(a) (b)

Figure 7- a) Experimental value of $\dot{Q}_h$ and T_i and simulated values. b) Difference between simulated and experimental inside temperature ($T_i - T_i^{EXP}$) for the refrigerated truck body.

All the dynamic states were initialized to their experimental value at the beginning of the test, making exception for the internal mass temperature T_{im}, which was initialized to the experimental value of the inside air temperature given the absence of a temperature measurement of the fan-heaters and evaporator, and the inside wall nodes, which were initialized by assuming a linear temperature profile between the internal and external surface at the beginning of the test.

The value of 8.7 W m^{-2} K^{-1} for the external surface heat transfer coefficient was calculated using a correlation for convection over a flat plate [33]; it is function of air velocity, which was assumed to be constant and equal to 2 m s^{-1} during the test. As for the value of the internal surface heat transfer coefficient, the value of 7.5 W m^{-2} K^{-1} was deduced from the measurements of the internal surface temperature during the experimental test and was found to be in accordance with the value of 8 $Wm^{-2}K^{-1}$ evaluated from Comini et al. [39].

3.3. Model validation and discussion

Experimental data were collected during a step test, performed in order to validate the optimum parameter set up, as described in Section 3. The temperature predicted by the model, compared with the experimental data collected during the step test is reported in Figure 8.

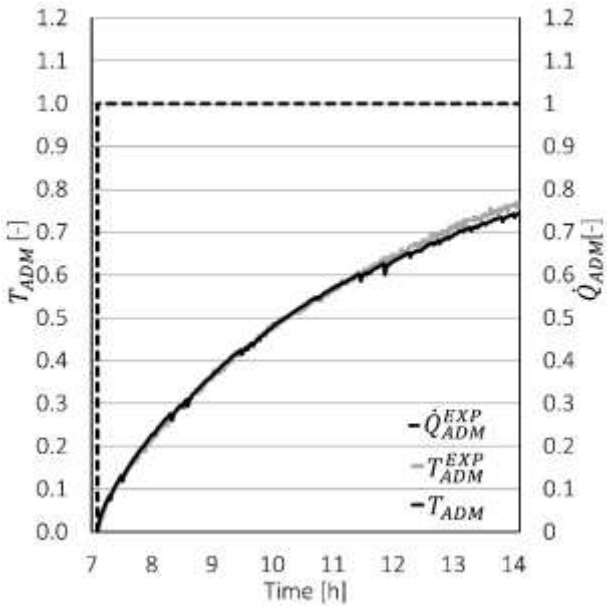

Figure 8- Step response of the system to a sudden increase of heating power.

The numerical model was able to well predict the dynamic evolution of the internal temperature, having a difference between the predicted temperature and the experimental temperature always below 0.1 °C.
While the results of the best fitting can be related to the nominal dimensions, as stated before, the direct characterization of the vehicle parameters from the average walls composition can lead to significant errors, as the thermal bridges and the structural components are ignored.
Table 4 shows the average wall composition data (av) in comparison with the best fit values (see Section 4.2 and Table 3).

Table 4: Comparison between global optimum wall parameters and the average wall composition data.

PARAMETER	DEFINITION	BEST FIT	av		Δ
C_w	Wall thermal capacity	632.3	333.28	kJ K^{-1}	47 %
R_w	Wall resistance	863 10^{-4}	1052 10^{-4}	K W^{-1}	-23 %

The best fit value of thermal mass is almost two times higher compared to the value obtained from the 2D wall characterization, as includes the additional mass inside the truck body envelope, i.e. wooden and metal localized reinforcements. This additional mass inside the truck body structure not only increases the value of thermal mass but also introduces thermal pairs and bridges, causing an overall reduction in thermal resistance.

4. Simulation results

The objective of this paper is to investigate on the dynamic behaviour of the insulated body of a refrigerated vehicle during a transport mission. The developed mission consists of a single day mission where the trucks have to travel from a distributor's premises to another.

The external conditions, i.e. the hourly ambient temperature, relative humidity and intensity of solar radiation are provided by the climate data available in Energy Plus [40]. A reference summer day of the standard climatic year of Athens has been chosen to represent a high load condition.
The refrigerated cargo is modelled as the internal mass of eq.9 and consists of 1000 kg bovine carcasses, having a specific heat capacity of 3.25 kJ kg^{-1} K^{-1} [41] and a convective heat transfer coefficient which is equal to 8 $Wm^{-2}K^{-1}$ [42] during transport operation.

4.1. Mission definition

Mission was designed to reproduce a long-distance delivery, and is described by setting the vehicle speed, the state of the cooling system (operating or not), the opening of the doors and the fraction of the prescribed cargo. Mission variables are reported in Figure 9.
Precooling operation must take place before the mission: the air inside of the insulated body is pulled down to its set point value for long enough to reach a steady state condition. After the precooling operation, the refrigerated vehicle is loaded with the refrigerated cargo. During loading (and unloading) operation, the cooling unit is kept off and the insulated box is put in contact with a controlled environment at $T_{amb} = T_i^{set}$ (thus nullifying the thermal load given by the leakage flow), since the goods are loaded into the enclosure directly from a cold store, where they had been precooled. In order to make the simulated mission as real as possible, at least stop must be planned. During stops the cooling unit is assumed to be active. On the other hand, when the refrigerated vehicle is parking at the owner's premises and empty, the cooling unit is kept off.

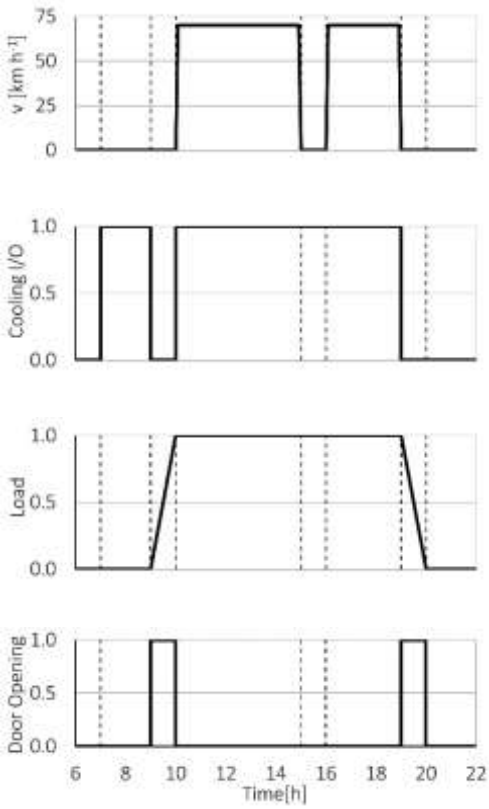

Figure 9- Mission profile; a) velocity; b) cooling unit operation time; c) cargo fraction; d) door opening time.

Initial conditions of the model were obtained by simulating the empty truck still under the variable ambient conditions for a time long enough for the solution to be independent from the initial conditions. Simulations were run to discuss the thermal dynamic loads of the truck during the mission. These results are reported in section 5.2. the outcomes of the model are compared to the results obtained with an algebraic model, which neglects the box inertia and the dynamic behaviour (section 5.3). Finally, the model was then used to assess the impact of the external walls solar adsorption coefficient on the average consumption (section 5.4).

4.2. Reference vehicles results.

The simulation model allowed to identify how the dynamic load and the mission profiles affect the actual cooling power demand inside the truck. Three fluxes were chosen to describe the system behaviour: the cooling power demand $\dot{Q}_c$ (see Section 4.1), the conduction flux between the internal and the external surface of the box $\dot{Q}_{cnd} = \frac{1}{\mathrm{R_w}}(T_{es} - T_{si})$, and the thermal load on the external surface given by the ambient conditions $\dot{Q}_e = \dot{Q}_{conve} + \dot{Q}_{rad}$, which can be obtained as the sum of the convective, $\dot{Q}_{conve} = \alpha_e S_e (T_{amb} - T_{es})$, and of the radiating fluxes (Eq.10). All these fluxes are reported in Figure 10.

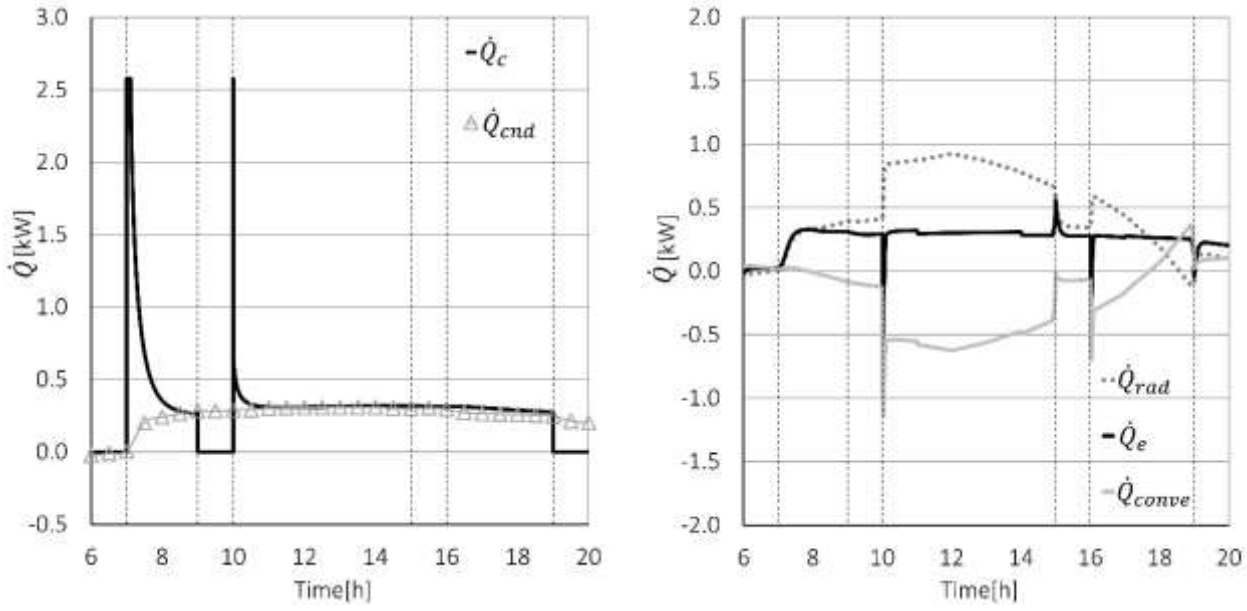

(a) (b)

Figure 10- a) Cooling power demanded by the insulated body and conductive flux through the walls. b) External heat fluxes during the mission.

Figure 10a compares the conduction flux between the interior and the exterior of the insulated box and the cooling demand of the refrigerating system. The average heat conduction is quite constant during the day, and approximatively equal to 300 W. The cooling demand flows closely this value, except between 7:00 to 8:00 and 10:00 to 11:00, when the refrigeration unit is cooling the air inside of the box to the set value. Despite the refrigeration unit is oversized and can provide a much larger power than the average conduction load, which for the considered mission is 253 W, the pull-down time at the beginning of the mission is significant (75'), justifying the sizing proposed by the commercial catalogues for a similar truck body. While the conduction heat flow through the box walls is quite constant, the fluxes on the external side of the wall change significantly during the mission, as reported in figure 10b. Radiation and convection act for the great

part of the day counterbalancing each other: the solar radiation increases the surface temperature above the ambient temperature; this leads to an increase both in the convective and in the radiative exchange with the ambient, although the two contributes have different signs.

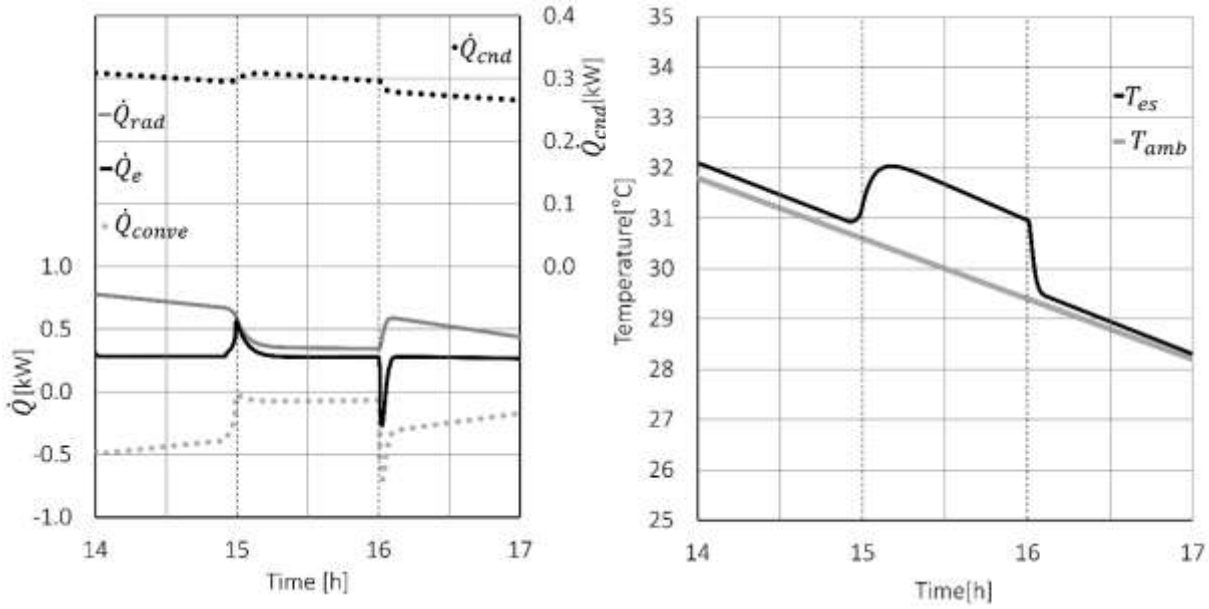

(a) (b)

Figure 11- a) Radiation and convective heat transfer rate. b) External wall temperature.

Figure 11 details the heat flux and the temperatures on the external wall between the 14:00 and the 17:00. When the vehicle is moving the external wall temperature (T_{es}) reaches its equilibrium at about +0.3°C above the ambient temperature (Figure 11b). On the other hand, when the vehicle is not moving (15:00 – 16:00) the solar radiation heat transfer ($\dot{Q}_{rad}$) becomes dominant over convection ($\dot{Q}_{conve}$) leading to a new equilibrium at +1.7 °C, as visible in Figure 11b. The peak in the net external flux $\dot{Q}_e$ at 15:00 is related to the wall thermal capacity, thus not impacting on the conduction flux: the trend of the conductive heat through the box walls is visible in Figure 11(a), increasing its value by 13 W and reproducing the same trend of the external wall temperature T_{es}.

4.3. Comparison between a mass and a mass-less model

The thermal mass of the walls of a refrigerated vehicle determines the amount of thermal energy which may be stored within the structure and provides the thermal inertia against the external temperature fluctuations, making it an important characteristic for transient thermal behaviour. In order to make considerations on the effect of thermal mass on the cooling energy required during the mission and on the dynamic load, the results of a wall-massless model (obtained by imposing C_j=0 (j=1…11) on eqs. 5-9 are considered.

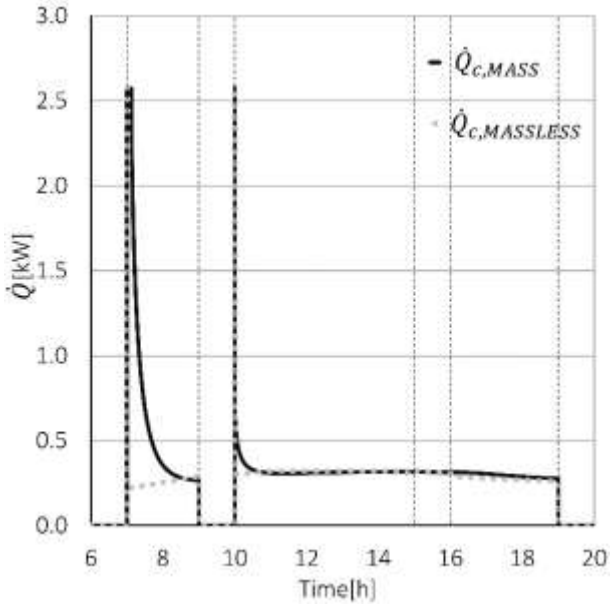

Figure 12- Comparison between the demanded cooling power by the mass and massless model.

Figure 12 provides the comparison between the cooling power required by the body truck as resulting from the mass and massless model. The main difference between the power trends can be seen during the pull-down operations: while the massless-model begins to modulate the cooling demand almost immediately, the modulation of the cooling power required by the mass-model takes about 75 minutes. This is due the fact that the mass model must also extract the heat stored into the walls and the dynamic response of the system is highly influenced by the thermal inertia, which is obviously not present on the massless-model. Consequently, the cooling energy demand resulting from a massless model will be smaller than the cooling energy demanded obtained with a model that considers the mass of the walls: in this case, it was found to be 25% lower. Simulations show that, while during the mission the cooling power required by the insulated body resulting from the two models is pretty much the same (h.11-h.19), a huge difference between the dynamic behaviour can be noticed during the pull-down operation.
In general terms, in a complete mission analysis, the adoption of a massless model would result in neglecting pull down operations following the inactivity of the trucks, for instance during week end, or door opening in uncontrolled environment, for example for loading or unloading operations or deliveries. As the pull-down plays a major role in the total cooling energy requirement, using a massless model would lead to a significant error in the evaluation of energy consumption, making clear that the thermal mass of the walls in a transient simulation is essential.

4.4. Influence of the surface absorption coefficient,a_s

In order to reduce the load imposed by the solar radiation, the insulated body's external wall should be characterized by a low value of solar absorption coefficient. Ageing and soiling of the insulated body could lead some increase of this coefficient. Furthermore, branding and other non-technical motivation can lead to the choice of externally coloured surface, increasing the absorption coefficient even in brand new and clean trucks.

To study the influence of the solar absorption coefficient on the cooling demand of the insulated body, three different values were considered:

- a_s=0.15, for a clean white external surface [36].
- a_s=0.50, assumed value for a very dirty white external surface.
- a_s =0.9, assumed value for painted black external surface.

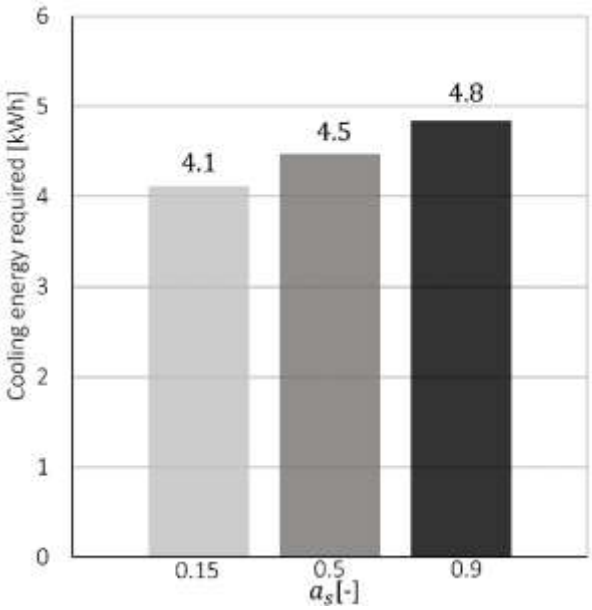

Figure 13- Cooling energy demand of the insulated boxes during the mission for three different values of solar absorption coefficient.

Figure 13 reports for the three cases the cooling demand required by the insulated box to complete the considered mission. With a solar absorption coefficient equal to 0.5 instead of 0.15, the cooling energy demand increases by 8% while if the solar absorption coefficient is equal to 0.9 instead of 0.15 the increase of cooling energy demand corresponds to 15%. This increase is due to the overheat of the walls during the mission caused by a higher radiation heat transfer absorbed by the wall itself.

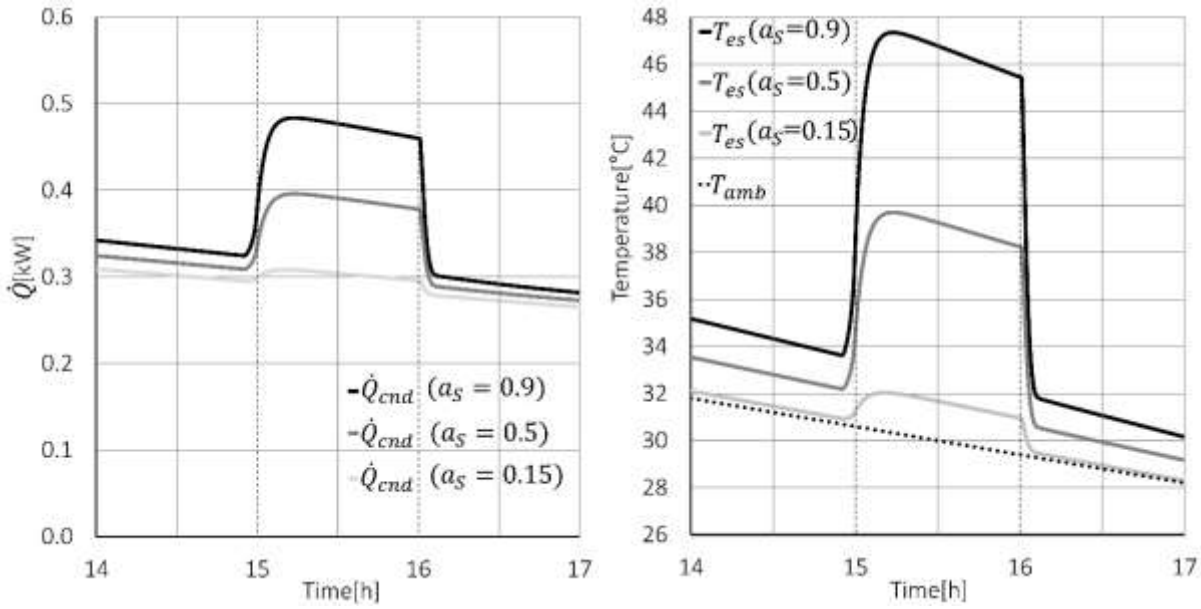

(a) (b)

Figure 14- Trend during the stop time of the reference vehicle for 3 different values of solar absorption coefficient of a) conductive flux through the walls and b) external surface temperature.

The overheat of the walls due to a higher value of solar absorption coefficient can be seen in Figure 14 for both conduction heat load and external wall temperature. When the vehicle is moving, the turbulent convective coefficient is high enough to allow an almost complete rejection of the solar heat flux to the ambient with small temperature difference ($T_{es} - T_{amb} \cong 0.3$ °C), thus reducing the impact of different radiation load on the conductive flux (figure 14a for Time < 15:00 hr. and Time > 16:00 hr.). On the other hand, when the vehicle is stopped (hr. 15:00-16:00), the decrease in the convection coefficient leads to a higher overheating and higher sensitivity to the solar absorption coefficient. Due to the increase of the absorption coefficient from 0.15 to 0.9, the cooling energy increases by 8% (see Fig. 13) but the conduction heat flowrate increases by 57% (see Fig.14).

5. Conclusions

This paper evaluates the possibility of describing a real truck insulated body by a 0D lumped model and to evaluate the impact of the environment and mission on the actual cooling demand. Experimental data from ATP test were used to train the model, which was then validated with a further dataset measured during a step test.

The dynamic model is able to correctly predict the thermal response of the insulated body to an external solicitation, which is of crucial importance during the dimensioning and sizing of a cooling unit in refrigerated transport applications. The numerical model was achieved by formulating a 0-dimensional lumped capacity method, which is one of the simplest and computationally most efficient method utilized in the study of the transient thermal behaviour. The model validation showed a good agreement between simulated results and experimental data, with a maximum difference in the predicted average internal temperature equal to 0.3°C. These are the main results:

1. The first important result was obtained during the numerical tuning of the dynamic model: it was found that the overall thermal capacity as well as the insulation characteristics cannot be derived from the stratigraphy of the wall: they would provide a rough approximation which can lead to significant errors. The best-fit value of thermal capacity was found to be 47% higher than the one derived from stratigraphy while the best-fit value of thermal resistance was evaluated by 23% lower than the one obtained by stratigraphy.
2. The simulation model allowed to identify how the dynamic load and the mission profiles affect the actual cooling power demanded by the refrigerated space during the mission: it was possible to see that the average heat conduction through the walls of the insulated body was quite constant during the day, with a value of 300 W, while the cooling power followed it closely, except for the times when the refrigeration unit had to cool down the air inside the box and inner cladding of walls to the set value. Radiation and convection heat flowrates over the external surface of the insulated body varied significantly during the mission when the truck is moving, counterbalancing each other for the great part of the day.

3. This study provided a sensitivity analysis of the model to the solar absorption coefficient a_s, by considering the simulation of the same mission with 3 different value of solar absorption coefficient for a cleaned white surface, very dirty white surface and a black painted surface. It was possible to find a maximum increment of 15% for the cooling energy demand when the external black surface body was considered. Eventually, the dependence of the model from the thermal mass of the walls was studied: results provided by a mass and a massless model were compared finding that, while the energy (power) required during the pull-down operation is much lower for a massless model, the peak of cooling demand and the mean cooling demand during the mission are pretty much the same.
4. The present study suggests a first theoretical step towards a better understanding and prediction of the dynamic thermal behaviour of the insulated body of a refrigerated vehicle, which is of crucial importance to minimize the energy consumption during a mission. The method proposed in this work gives also a substantial improvement in modelling performance with a negligible increase of computer effort, since it utilizes a low-order lumped capacity method. It also evaluates the heat flowrates and the cooling energy required by the insulated body during a mission, while maintaining the set-point temperature.

In order to discuss more complex and general missions and to relate the mission profile to the cooling unit energy performance and control strategy, further developments may include:

1. dynamic simulation of a cooling unit, the dynamic of the internal air as effect of the unit cycles, door opening, load lay-out and vehicle speed changes;
2. simulation of coupled heat and mass transfer phenomena during a mission, given by door opening operations in a non-controlled environment (i.e. external ambient conditions) which will cause not only a temperature variation but also a variation in relative humidity inside of the insulated truck body. This will allow to include dehumidification process on the cooling unit model and frost formation/defrost cycling;
3. detailed simulation of heat transfer and heat generation phenomena that can be significant for some type of perishable foodstuff such as vegetables and fruits, which might be loaded at harvest temperature.

Appendix 01

Table A1: constituting elements of the vehicle's walls.

Type of wall	**Constituting elements**
Lateral wall	Fiberglass: 1.5 mm Polyurethane: 67 mm Fiberglass: 1.5 mm
Floor	Fiberglass: 1.5 mm Plywood plate: 18 mm Polyurethane: 79 mm Fiberglass: 1.5 mm
Roof	Fiberglass: 1.5 mm Polyurethane: 97 mm Fiberglass: 1.5 mm
Front wall	Fiberglass: 1.5 mm Polyurethane: 67 mm Fiberglass: 1.5 mm
Rear wall	Fiberglass: 1.5 mm Polyurethane: 67 mm Fiberglass: 1.5 mm

References

[1] S.A. Tassou, G. De-Lille, Y.T. Ge. Food transport refrigeration - approaches to reduce energy consumption and environmental impacts of road transport. Applied Thermal Engineering, Elsevier, 2009, 29 (8-9), pp.1467.

[2] M. Ahmed, O. Meade, M.A. Medina, 2010, reducing heat transfer accords the insulated walls of refrigerated truck trailers by the application of phase change materials. Energy Covers. Manag.51, 383-392.

[3] UNEP. Report of the Refrigeration, Air conditioning and Heat Pumps Technical Options Committee, 2010.

[4] Total number of relevant goods vehicles in the reporting countries, 2012-2016, Eurostat, https://ec.europa.eu/eurostat/statistics-explained/index.php?title=File:Total_number_of_relevant_goods_vehicles_in_the_reporting_countries,_2012-2016.png

[5] United Nations, Agreement on the international carriage of perishable foodstuffs and on the special equipment to be used for such carriage (ATP), UNECE Transport Division, Geneva, Switzerland, 1970.

[6] S.K. Chatzidakis, K.S. Chatzidakis, Refrigerated Transport and Enviroment, 2003. Available from : <http://www3.interscience.willey.come/cgi-bin/fulltext/109060950/PDFSTART/>.

[7] TRANS/WP.11/2000/9, Economic Commission for Europe, Inland Transport Committee, Working Party on the Transport of Perishable Foodstuffs (Geneva, 30 October- 2 November 2000), Comment to Annex 1, Appendix 2, paragraph 29, Transmitted by the expert from Denmark. Available from: <http://unece.org/trans/wp11/wp11doc/2000/wp110009.pdf/>.

[8] S. Estrada-Flores, A. Eddy. Thermal performance indicators for refrigerated road vehicles, International Journal of Refrigeration, 29, (2006) 889-898.

[9] M. Kayfeci, A keçebas, E. Gedik, Determination of optimum insulation thickness of external walls with two different methods in cooling applications, Appl. Thermal. Eng., 50 (2013), pp. 217-224.

[10] R. Derrek, J. Bloemhof, I. Mallidis, 2012. Operations research for green logistics- an overview of aspects, issues, contributions and challenges. Eur.j.Oper.Res.219(3), 671-679.

[11] O. Adekomaya, T. Jamiru, R. Sadiky, Z. Huan, 2016. Sustaining the shelf life of fresh food in cold chain- a burden on the environment. Alexandria Eng. J. 55(2), 1359-1365.

[12] International Institute of refrigeration,16th Informatory Note on Refrigeration, refrigerated transport: progress achieved and challenges to be met. Available from: <http://www.iifiir.org/userfiles/file/publications/notes/NoteTech_16_EN.pdf>, 2003, p.1.

[13] James, S.J., C. James, and J.A. Evans. 2006. Modelling of food transportation systems—a review. International Journal of Refrigeration 29(6):947–57.

[14] P.G. Jolly, C.P.Tso, Y.M. Wong, S.M Ng, Simulation and measurement on the full-load performance of a refrigeration container system in a shipping container, International Journal of Refrigeration 23(2000) 112-126.

[15] Li B, Otten R, Chandan V, Mohs WF, Berge J, Alleyne AG (2010) Optimal on-off control of refrigerated transport systems. Control Eng Pract 18(2010):1406–1417.

[16] Bin Li, Neera Jain, William F. Mohs , Scott Munns , Vikas Patnaik , Jeff Berge & Andrew G. Alleyne (2012) Dynamic modeling of refrigerated transport systems with coolingmode/heating-mode switch operations, HVAC&R Research, 18:5, 974-996.

[17] Tso C. P., Wong Y. W., Jolly P. G., and Ng S. M., 2001, “A comparison of hot-gas by-pass and suction modulation method for partial load control in refrigerated shipping containers,” Int. J. Refrig., 24, pp. 544–553.
[18] Chatzidakis, S. K., Athienitis, A. and Chatzidakis, K. S. (2004), Computational energy analysis of an innovative isothermal chamber for testing of the special equipment used in the transport of perishable products. Int. J. Energy Res., 28: 899-916.
[19] S.K. Chatzidakis, K.S. Chatzidakis, A heat transfer simulation study of a multi-compartment isothermal liquid foodstuff tank tested according to the international ATP agreement, Energy Conversion and Management 46(2) (2005) 197-221.
[20] S. Estrada-Flores, D.J. Tanner, N.D. Amos, Cold chain management during transport of perishable products, Food Australia 54(7) (2002) 268-270.
[21] N. Amos, D.J. Tanner, Temperature variability during refrigerated vessel shipment of fresh produce, in : Porceedings of the 21st International Congress Refrigeration, 2003, ICR 0250, 8 pp.
[22] D.J. Tanner, N.D. Amos, Temperature variability during shipment of fresh produce, Acta Horticulturae 599 (2003), 193-203.
[23] N.J. Smale, J. Moureh, G. Cortella, A review of numerical models of airflow in refrigerated food applications, International Journal of Refrigeration, Volume 29, Issue 6, 2006, Pages 911-930.
[24] Han, J. , Zhao, C. , Yang, X. , Qian, J. and Xing, B. (2016), Computational Fluid Dynamics Simulation to Determine Combined Mode to Conserve Energy in Refrigerated Vehicles. J Food Process Eng, 39: 186-195.
[25] C.P. Tso, S.C.M. Yu, H.J. Poh, P.G. Jolly, Experimental study on the heat and mass transfer characteristics in a refrigerated truck, Int J Refrigeration 25 (2002) 340-350.
[26] J. Moureh, N. Menia, D. Flick, Numerical and experimental study of airflow in a typical refrigerated truck configuration loaded with pallets, Computers and Electronics in Agriculture 34 (2002) 25-42.
[27] J. Moureh, D. Flick, Airflow pattern and temperature distribution in a typical refrigerated truck configuration loaded with pallets, International Journal of refrigeration 27 (2004) 464-474.
[28] M. Tapsoba, J.Moureh, D.Flick, Airflow pattern in an enclosure loaded with pallets: the use of air ducts, Eurotherm seminar 77, Heat and Mass transfer in Food Processing, June 20-22, Parma, Italy, 2005.
[29] Estrada-Flores, S. Evaluation of dynamic models for refrigeration system components: a thesis presented in partial fulfilment of the requirements for the degree of Doctor of Philosophy in Process and Environmental Technology at Massey University.
[30] Estrada-Flores, S., Cleland, A. C., & Cleland, D. J. (1995, August 20-25). Modelling of thermal behaviour of walls for low temperature applications: sandwich panel type. Paper presented at the 19th International Congress of Refrigeration, The Hague, Netherlands.
[31] Estrada-Flores, S. and Eddy, A. The use of thermography to aid design of refrigerated road vehicles. Proc. "Innovative Equipment and Systems for Comfort and Food Preservation", 2006. International Institute of Refrigeration. Auckland, NZ.
[32] Carrier. Light commercial vehicle refrigeration unit < https://www.carrier.com/truck-trailer/en/it/products/it-truck-trailer/lcv/pulsor-300/> , 2018, p.1.
[33] ASHRAE. ASHRAE Fundamentals Handbook (SI), Chapter4, 2009.
[34] ASHRAE. ASHRAE handbook: HVAC applications. Atlanta (GA): ASHRAE, 1999.
[35] United States Department of Energy (DOE): EnergyPlus Engineering Reference Version 8.2: The Reference to EnergyPlus Calculations. The Reference to EnergyPlus Calculations, 2015, p.92-94.

[36] S. Rossi, P. Bison, A. Bortolin, G. Cadelano, G. Ferrarini, A. Libbra, A. Muscio. In field evaluation of the absorption coefficient of the external surface of the insulated box in a refrigerated vehicle. Proceedings of the 2nd IIR International Conference on Sustainability and the Cold Chain, Paris, April 2013.
[37] T Lafaye de Micheaux, M Ducoulombier, J Moureh, V Sartre, J Bonjour. Experimental and numerical investigation of the infiltration heat load during the opening of a refrigerated truck body. International Journal of Refrigeration, Elsevier, 2015.
[38] Kramer R., Schijndel J., Schellen H.,Simplified thermal and hygric building models: A literature review, Frontiers of Architectural Research,Volume 1, Issue 4,2012,p. 318-325.
[39] G.Comini, G.Cortella, O.Saro, Finite element analysis of coupled conduction and convection in refrigerated transport, International Journal of Refrigeration 18: 123-131,,1995.
[40] Energy Plus Weather Data, EnergyPlus. <https://energyplus.net/weather location/europe_wmo_region_6/GRC//GRC_Athens.167160_IWEC >.
[41] ASHRAE. 2006. Refrigeration Handbook, Chapter R09, Thermal properties of foods. Atalanta, GA, USA: American Society of Heating, Refrigerating and Air-Conditioning Engineers.
[42] Harris, M. B., Carson, J. K., Willix, J., & Lovatt, S. J. (2004). Local surface heat transfer coefficients on a model lamb carcass. Journal of Food Engineering, 61, 421-429.

Nomenclature

a_s	Surface absorptivity [-]
C	Lumped thermal capacity [J kg^{-1} K^{-1}]
e	Error between the feedback temperature and the setpoint temperature [°C]
H	Height [m]
I	Intensity of solar radiation [W m^{-2}]
$\hat{k}$	Normal vector toward sky globe [-]
k	Proportional gain [-]
K	Global heat transfer coefficient [$Wm^{-2}K^{-1}$]
L	Length [m]
MSE	Mean square error [-]
N_{wall}	Number of wall nodes [-]
$\hat{\mathbf{n}}$	Normal vector toward surface orientation [-]
$\dot{Q}$	Heat flux [W]
R	Thermal resistance [K W^{-1}]
S	Surface [m^2]
T	Temperature [°C]
t	Time [s]
V	Volume [m^3]
$\dot{V}$	Air volumetric flowrate [m^3 s^{-1}]
W	Width [m]

Greek symbol

α	convective heat transfer coefficient [$Wm^{-2}K^{-1}$]
δ	thickness [m]
ε	wall emissivity coefficient [-]
ρ	density [kg m^{-3}]
σ	Stephan-Boltzmann constant [W m^{-2} K^{-4}]
τ	integral gain [-]

Exponent

av	average wall thickness composition
EXP	experimental
set	set-point

Subscript

ADM	non-dimensional
amb	ambient
c	cooling
cnd	conduction
conv	convection
e	external
dir	direct component of solar radiation
diff	diffusive component of solar radiation
es	external surface
h	heating
i	internal
im	internal mass
inf	infiltration
is	internal surface
max	maximum
nom	nominal
rad	radiation
sky	sky
ss	steady state condition
w	wall

HIGHLIGHTS:

1) Development of a dynamic model to study the thermal response of the insulated box.
2) Evaluation of the dynamic behavior of the insulated box during a typical mission.
3) Thermal capacity and thermal resistance cannot be derived from stratigraphy.
4) Numerical model was able to well predict the evolution of the internal temperature.
5) Mission was designed to reproduce a long-distance delivery.
6) Simulation model allowed to identify dynamic load and cooling power demand of the truck.